university of groningen / faculty of science and engineering

# Analysis of the invariant mass resolution of $e^+e^-$ pairs in $\Lambda_b^0 \to \Lambda^0 e^+e^-$ decays before and after the upgrade of the LHCb experiment

## Bachelor Research Project Physics 2022


*Author:*
Sander Bouma
S3772721

*Supervisors:*
Maarten van Veghel
Mick Mulder



**Abstract**

In order to use the $\Lambda_b^0 \to \Lambda^0 e^+e^-$ decay as a probe for LFU, it needs to be possible to distinguish this decay mode between other decay modes with the same decay products. This is done by the reconstruction of the invariant mass of $e^+e^-$ pairs. In this thesis, an analysis is performed on the resolution of the invariant mass of these $e^+e^-$ pairs for both Run 2 and Run 3 of the LHCb, using MC simulated data. This is done by comparing the true momenta and invariant masses to the reconstructed momenta and invariant masses of $e^+e^-$ pairs in both runs. It was found that the resolution in Run 3 is worse by a factor of 1.25. and that there are more energy losses by a factor of 1.7. The bremsstrahlung reconstruction for Run 3 has improved, as there are 12% more electrons reconstructed with on average a higher accuracy by a factor of 2.1.


July 8, 2022

## Acknowledgements

I would like to thank my supervisors Maarten van Veghel and Mick Mulder for providing me with the Run 2 and Run 3 data as well as their valuable support and insight. I really appreciate their help and their willingness to answer all of my questions, even the dumb ones. Thank you Mick for having a meeting with me and helping me even from Mexico at 5:00 o'clock in the morning.

# Contents

**1 Introduction** **3**

**2 Theory** **4**
2.1 The Standard Model of Particle Physics . . . . . 4
2.2 Flavour changing currents . . . . . 5
2.3 Probing lepton flavour universality . . . . . 5
2.4 $\Lambda_b^0$ decay as candidate for LFU probing . . . . . 6
2.5 Invariant mass . . . . . 7

**3 The LHC & the LHCb experiment** **8**
3.1 The LHCb detector . . . . . 9
3.2 Bremsstrahlung . . . . . 11

**4 Analysis & Results** **12**
4.1 Momentum cut . . . . . 13
4.2 Reconstruction of the di-electron invariant mass . . . . . 14
4.3 Resolution of the di-electron invariant mass . . . . . 15
4.4 Resolution of $e^{\pm}$ momenta . . . . . 17

**5 Discussion** **20**

**6 Conclusions** **21**

**References** **22**

**Appendix** **23**

# 1 Introduction

For centuries, physicists have been trying to understand the workings of Nature and have been exploring it beyond the reach of our senses, in search of what the fundamental building blocks of our Universe are and how they behave. So far, this has lead to the successful theory called the Standard Model (SM). The SM predicts precisely how the fundamental particles and forces behave and interact (aside from gravity). However, this model is incomplete. It is unable to explain the phenomena of Dark Matter, the abundance of matter over antimatter in our Universe, or explain the patterns seen in the interaction strengths of particles, as the SM does not agree with decay measurements of $b \to c\tau\nu_\tau$ and $b \to sl^+l^-$ transitions [1].

One method to test the SM and search for new physics is to test the properties of hadron decays and compare them with their corresponding SM predictions. By looking at $b$-hadron decays (particles containing a beauty-quark) the LHCb Collaboration found evidence for the breaking of lepton flavour universality (LFU) with a significance of 3.1 standard deviations [2]. LFU is the property that all types of charged leptons (electrons, muons, taus) interact in the same way with force mediators. Specifically, the LHCb Collaboration looked at the $B^+ \to K^+l^+l^-$, $\Lambda_b \to pK^-l^+l^-$ and $B^0 \to K^{0*}l^+l^-$ decays. Although, more evidence is needed to conclusively say whether LFU is broken in these decays or not.

Another testing ground for LFU is the $\Lambda_b^0 \to \Lambda^0 l^+l^-$ decay. The advantage with $\Lambda_b^0 \to \Lambda^0 l^+l^-$ is that both $\Lambda_b^0$ and $\Lambda^0$ can be polarised, which extents the number of angular observables and provides possibilities for additional tests of the SM [3]. However, decays such as $B \to Ke^+e^-$ and $\Lambda_b^0 \to \Lambda^0 e^+e^-$ are difficult to reconstruct due to the interactions of the di-electron pair with the detector material. To analyse these decays for LFU it needs to be possible to reconstruct the decay products with high enough precision. In this thesis, using simulated data the invariant mass of the $e^+e^-$ pair from the $\Lambda_b^0$ decay is reconstructed for both Run 2 and Run 3 of the LHC. This provides validation whether the $\Lambda_b^0 \to \Lambda^0 l^+l^-$ decay is a possible candidate for further analysis of LFU.

In coming years, more data for these decays will be gathered as Run 3 of the Large Hadron Collider (LHC) has started in July 2022. Prior to Run 3, the LHCb has received several upgrades, which make it possible to have a higher data readout, have more collisions and reconstruct the resulting particles with higher precision. For electrons specifically, the upgrade is supposed to better reconstruct their energy losses, because of improvements in the bremsstrahlung recovery algorithm.

In this thesis an overview of the Standard Model and lepton universality is given. The LHC and the LHCb experiment will be discussed as well as the upgrades for Run 3. Lastly, the resolution of the invariant mass of the $e^+e^-$ pair in the $\Lambda_b^0 \to \Lambda^0(\to p\pi^-)e^+e^-$, as well as its antimatter counterpart, are analysed and discussed.

# 2 Theory

## 2.1 The Standard Model of Particle Physics

With the rise of Quantum Mechanics in the 20$^{\text{th}}$ century and improvements in experimental resolution, scientists were able to investigate smaller and smaller structures of Nature and their dynamics. Physicists were able to put together a coherent picture of elementary particle physics which is known as the Standard Model (SM). The SM incorporates three of the four known fundamental interactions: the strong, weak and electromagnetic interaction, as well the types of particles that can feel these interactions, which make up matter. Of these particles, the most fundamental are the quarks and leptons. These, together with the force carrier bosons, appear to be point-like, having no internal structure. Six different types, or flavours, of quarks are known which come in pairs known as *generations*:

$$\begin{pmatrix} u \\ d \end{pmatrix}, \begin{pmatrix} c \\ s \end{pmatrix}, \begin{pmatrix} t \\ b \end{pmatrix}$$

Where the 'up'-type quark has a charge of $+\frac{2}{3}e$ and the 'down'-type quark has a charge of $-\frac{1}{3}e$. Each generation has an increase in particle mass. From these building blocks, other particles can be constructed. Bound states of quarks are called hadrons. Hadrons can then be divided into more categories: A baryon is a three-quark system, whereas a meson consists of a quark and an anti-quark. In addition to quarks, there are leptons which only interact weakly and electromagnetically. These also occur in three generations that have a one-to-one correspondence with the three quark generations:

$$\begin{pmatrix} \nu_e \\ e^- \end{pmatrix}, \begin{pmatrix} \nu_\mu \\ \mu^- \end{pmatrix}, \begin{pmatrix} \nu_\tau \\ \tau^- \end{pmatrix}$$

The three different types of leptons, electrons, muons and taus, have a separate neutrino $\nu_e$, $\nu_\mu$, $\nu_\tau$. In addition to these particles, each particle has its own anti-particle which has the opposite quantum numbers.

The forces between leptons and quarks are mediated through gauge fields and their corresponding gauge bosons. The $\gamma$ particle mediates the electromagnetic interaction, the $W^\pm$ and $Z^0$ boson mediate the weak interaction and the eight gluons $g$ the strong interaction. The SM has been supplemented by the discovery of the Higgs particle in 2012. This boson couples to mass and gives some of the fundamental particles their mass via the Higgs mechanism [4].

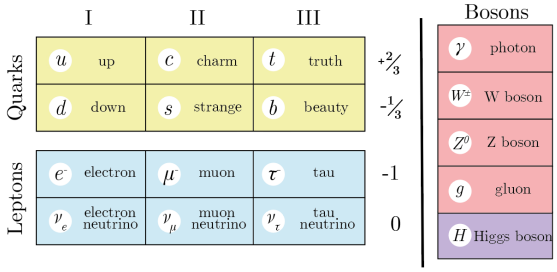


Figure 1: The Standard Model of Particle physics, showing each generation of matter and their charge, as well as the force carrier bosons and the Higgs boson.

## 2.2 Flavour changing currents

The stability of quarks in hadrons, like the stability of protons in nuclei, is influenced by their interaction energies. The interaction energies of quarks are governed by quantum chromodynamics (QCD) effects, which give the $s$, $c$, and $b$ quarks approximate lifetimes of $10^{-8}$ to $10^{-10}$ s for the $s$ quark and $10^{-12}$ to $10^{-13}$ s for $c$ and $b$ quarks [5]. Quark decay is governed by the weak interaction and proceeds by the exchange of a $W^{\pm}$ boson. By this flavour changing charged current (FCCC) process, the flavour of the quark is changed. These flavour transitions between quarks are encoded in the SM through the Cabibbo–Kobayashi–Maskawa (CKM) matrix [6]. In these interactions an 'up'-type quark decays only into a 'down'-type quark or vice versa due to the exchange of the charge carrying $W^{\pm}$ boson.

There are however interactions possible that change the flavour of a quark without altering its electric charge. These flavour changing neutral current (FCNC) processes are forbidden by the SM at tree level and are only possible through electroweak loop Feynman diagrams. Because these decays are highly suppressed by the SM, they may receive significant contributions from new quantum fields that lie beyond the SM.

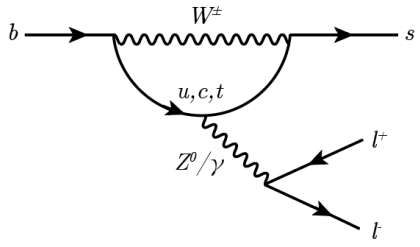


(a) $b \to sl^+l^-$ by an electroweak loop, allowed by the SM.

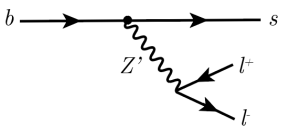


(b) $b \to sl^+l^-$ at tree level, by the exchange of a $Z'$ boson. Forbidden by the SM.

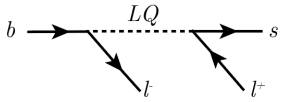


(c) $b \to sl^+l^-$ at tree level, by the exchange of a leptoquark. Forbidden by the SM.

Figure 2: Feynman diagrams of $b \to sl^+l^-$ transitions. Decay (a) shows the most significant SM contribution to this transition. Decays (b) and (c) are contributions allowed by theories beyond the SM involving or $Z'$ bosons or leptoquarks.

## 2.3 Probing lepton flavour universality

Lepton flavour universality (LFU) is a property emerging from the SM which states that all electroweak couplings of leptons to gauge bosons are independent of their flavour and only depend on their mass differences. In order to test LFU, branching fractions involving different lepton families are analysed for various decays. Of these, semileptonic decays of heavy hadrons are excellent candidates for testing LFU as in these decays all three generations can be accessed. Many models extending the SM contain additional interactions that could violate LFU. These are theories involving leptoquarks ($LQ$) [7] or $Z'$ particles [8]. Especially decays involving third generation quarks and leptons are interesting because many of these theories with LFU violation predict stronger coupling to the third generation of quarks and leptons [1]. These new particles could contribute to new interactions in quark transitions and their effect will be most significant in transitions suppressed by the SM. The main contributions to the $b \to sl^+l^-$ transition of these theories are shown in Fig. 2b and 2c.

For these reasons, ratios of $b \to sl^+l^-$ transitions for different lepton families provide excellent testing ground for LFU. Candidate decays include $B \to Hl^+l^-$ where $B = B^+, B^0, B_s^0$ or $\Lambda_b^0$ and $H$ a hadron or a combination of hadrons and $l^+l^-$ one type of oppositely charged leptons. The LFU testing ratio $R_H$ is defined as:

$$R_H = \frac{\int_{q^2_{min}}^{q^2_{max}} \frac{B \to H\mu^+\mu^-}{dq^2} dq^2}{\int_{q^2_{min}}^{q^2_{max}} \frac{B \to He^+e^-}{dq^2} dq^2}, \tag{1}$$

where $q^2$ is the invariant mass of the di-lepton pair squared. For the decays $B^0 \to K^{*0}l^+l^-$ and $B^+ \to K^+l^+l^-$ these ratios were found to be:

| Measurement | Result | $q^2$ region (GeV$^2/c^4$) | Significance | Ref. |
|---|---|---|---|---|
| $R_{K^+}$ | $0.846^{+0.042+0.013}_{-0.039-0.012}$ | $1.1 < q^2 < 6.0$ | $3.1\sigma$ | [9] |
| $R_{K^{*0}}$ (low-$q^2$) | $0.66^{+0.11+0.03}_{-0.07-0.03}$ | $0.045 < q^2 < 1.1$ | 2.1 - $2.3\sigma$ | [10] |
| $R_{K^{*0}}$ (high-$q^2$) | $0.69^{+0.11+0.05}_{-0.07-0.05}$ | $1.1 < q^2 < 6.0$ | 2.4 - $2.5\sigma$ | [10] |

Where the first error is statistical and the second one systematic.

Their SM predictions are $R_{K^+} \approx R_{K^{*0}} \approx 1$ within the order of 1% [11, 12]. Although these results do not confirm LFU violation in $b \to sl^+l^-$ transitions yet, they are all slightly below the SM predicted value of 1 and are thus in tension with their SM predictions. Further analysis is needed to conclusively say whether LFU is broken in these $b \to sl^+l^-$ transitions or not.

## 2.4 $\Lambda_b^0$ decay as candidate for LFU probing

Another candidate for LFU testing is the $\Lambda_b^0$ baryon. $\Lambda^0$ baryons are a type of hadron containing one up quark, one down quark and a third quark of a higher flavour generation. The $\Lambda_b^0$ baryon is an isospin-0 $udb$ state and can decay through the following process:

$$\Lambda_b^0 \to \Lambda^0(\to p\pi^-)l^+l^- \tag{2}$$

The SM predicts that the LFU testing ratio for this decay is $R_\Lambda = 1.000 \pm 0.003$. The $\Lambda_b^0 \to \Lambda^0 l^+l^-$ decay is an interesting candidate as the $\Lambda_b^0$ and $\Lambda^0$ can be produced polarised. This extents the number of angular observables of this decay from 10 to 34, which can result in a different measurement result of $R_\Lambda$ compared to $R_K$ [3].

The decay in Eq. 2 is however not the only decay that produces a $\Lambda^0$ and two leptons. Another decay proceeds as follows:

$$\Lambda_b^0 \to \Lambda^0(\to p\pi^-)J/\psi(\to l^+l^-), \tag{3}$$

where the $J/\psi$ meson is a $c\bar{c}$ resonance. The resolution of $R_\Lambda$ highly depends on the ability to distinguish between these two decay modes as well as other backgrounds. These decays however cannot be spatially distinguished by the detector, as the lifetime of the $J/\psi$ meson is in the order of $10^{-21}$ s. These decay modes can only be distinguished by the invariant mass of the dilepton pair.

## 2.5 Invariant mass

The invariant mass of the di-electron pair is defined as:

$$m_{ee} = \frac{1}{c^2}\left[\left(E_{e^-} + E_{e^+}\right)^2 - \left(\mathbf{p}_{e^-} + \mathbf{p}_{e^+}\right)^2 c^2\right]^{1/2}, \tag{4}$$

where $E_{e^\pm}$ and $\mathbf{p}_{e^\pm} = (p_x, p_y, p_z)$ are the energy and momentum of the electron respectively. If the observed decay proceeds according to Eq. 2, no peak is observed in the invariant mass spectrum, because the momenta of the two electrons are not directly correlated in this decay. If however the decay proceeds according to Eq. 3, then the two momenta are correlated through the intermediate $J/\psi$ resonance. In the invariant mass spectrum, a peak would be observed at the mass of this resonance. These peaks are also observed for other resonances such as the $\Psi(2S)$ resonance and the photon. A representation of these invariant mass distributions is shown in Fig. 3. By this method, the different decay modes of $\Lambda_b^0$ resulting in a $\Lambda^0$ and two leptons can be distinguished from each other.

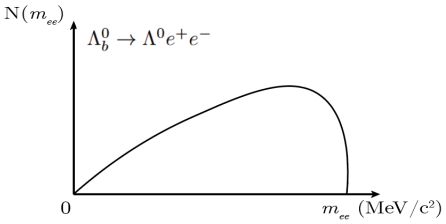


(a) Invariant mass distribution of $\Lambda_b^0 \to \Lambda^0 e^+ e^-$.

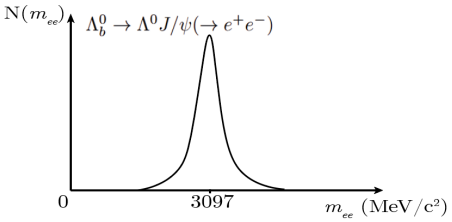


(b) Invariant mass distribution of $\Lambda_b^0 \to \Lambda^0 J/\psi(\to e^+ e^-)$.

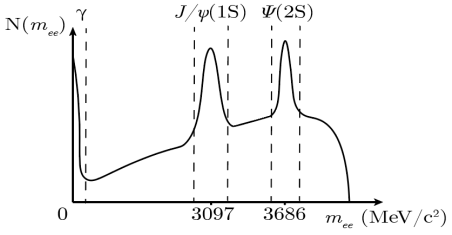


(c) Combinatory effects of $\Lambda_b^0 \to \Lambda^0 e^+ e^-$, $\Lambda_b^0 \to \Lambda^0 J/\psi(\to e^+ e^-)$, $\Lambda_b^0 \to \Lambda^0 \Psi(\to e^+ e^-)$, and $\Lambda_b^0 \to \Lambda^0 \gamma(\to e^+ e^-)$.

Figure 3: Invariant mass distributions of different $\Lambda_b^0$ decay modes, resulting in a $\Lambda^0$ and two electrons.

# 3 The LHC & the LHCb experiment

The beams inside the LHC are made to collide at four locations around the accelerator ring. These stations are ATLAS, CMS, ALICE and LHCb. The LHCb detector is designed to study $b$-hadron and $c$-hadron decays originating from $pp$-collisions (proton-proton collisions). The goal of the detector is to infer the four-momentum, the origin vertex and the type of particle of the particles created in the $pp$-collision. This data is then used to analyse various decay modes and look for physics beyond the SM.

The LHC has collided protons in sets of runs. Run 1 of the LHC ran from 2010 till the end of 2012 and during this time the collisions took place at a centre-of-mass energy of $\sqrt{s} = 7$ TeV. Run 2 began in the middle of 2015 and finished at the end of 2018, during which collisions took place at $\sqrt{s} = 13$ TeV. Run 3 has started in July of 2022, and collisions take place at $\sqrt{s} = 13.6$ TeV. The LHC provides $pp$-collisions to LHCb with a rate of 40 MHz, but for Run 3 the luminosity has been increased by almost a factor of 5. This is done by reducing the spread of the proton bundles in the LHC. The increase in luminosity is from $\mathcal{L} = 3 - 4 \times 10^{32}$ cm$^{-2}$ s$^{-1}$ to $\mathcal{L} = 1 - 2 \times 10^{33}$ cm$^{-2}$ s$^{-1}$. With the higher luminosity, more collisions will take place in the detector. The detector is expected to collect a sample of 50 fb$^{-1}$ over a course of 10 years.

In Run 2, the LHCb generated an amount of data equivalent to 1 TB per second, which is too much to store. With the increase in luminosity, this rate has also gone up by almost a factor of 5. In both runs, numerous methods are used to significantly reduce the data without losing data quality. Data from the detector are filtered through the *trigger*, which consists of the Level 0 hardware trigger (L0) and the High Level Trigger (HLT). The main difference in data acquisition between Run 2 and Run 3 is the removal of the L0 hardware trigger, as it limited the data readout. In Run 3, data is read out at the full 40 MHz and is filtered only through the HLT in the software.

## 3.1 The LHCb detector

Compared to the general purpose detectors like ATLAS or CMS, the LHCb detector has quite a different geometry. Whereas CMS and ATLAS completely surround the collision point, the LHCb detector is a forward spectrometer of conical shape. This is justified by the fact that at high energies, both $b$- and $\bar{b}$-hadrons are predominantly produced in the forward or backward cone. The LHCb detector is placed on one side of the collision point, surrounding the beam line. It has dimensions of 20 m long, 10 m high and 13 m wide. A schematic overview of the detector is shown in Fig. 4. During Long Shutdown 2 of the LHC from 2018 to 2022, the LHCb detector has received several upgrades, with the major changes being the VELO, the tracking stations and the data readout [13]. The main goal of these upgrades is to maintain performance at higher luminosities and to collect more data. For electrons specifically, the upgrade is expected to have a higher reconstruction efficiency due to improvements in the recovery of their energy losses.

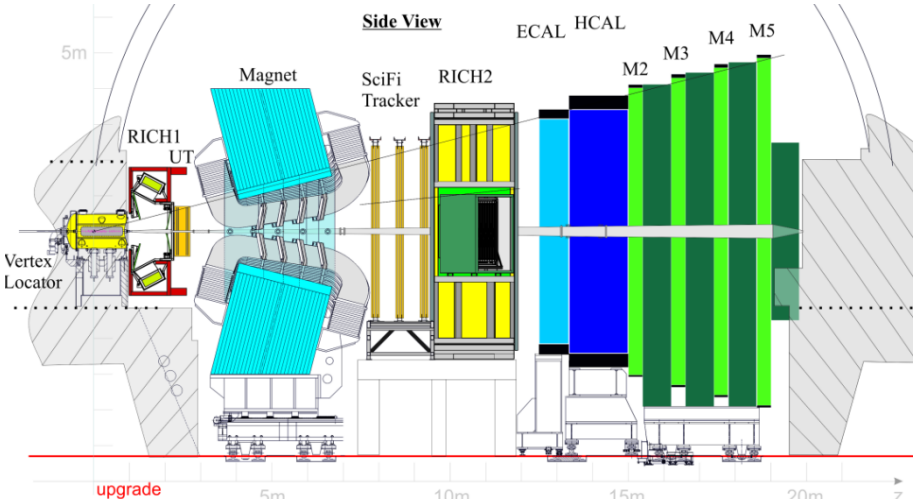


Figure 4: Overview of the LHCb detector used for Run 3, with each subdetector and its scale [13].

The VELO (vertex locator) is the first detection instrument and is used to reconstruct the primary vertices and decay vertices using precise measurements of the particle's decay products. The VELO consists of a series of two movable halves that get within a distance of a couple of millimeters to the beam. This is necessary, since the particles of most interest have a lifetime in the order of $10^{-12}$ s and hence only travel a few millimeters before decaying. The upgraded VELO uses hybrid pixel silicon detector modules with microchannel cooling and can get within 3.5 mm to the beam, whereas the previous VELO consisted of silicon microstrip sensors and could only get within 5 mm of the beam. Multiple modules with these sensors are placed in an array along the beam-axis. By measuring the location of particle hits on each module, a set of tracks can be reconstructed to find the locations of the decay vertices.

The rest of the tracking system consists of a 4 Tm dipole magnet with tracking detectors both upstream and downstream of the magnet. This system provides a high precision estimate of the momentum of charged particles. Their reconstructed trajectories are used as inputs for the RICH detectors.

The region between the VELO and the dipole magnet is instrumented with a large area silicon strip detector, called the Upstream Tracker (UT). The main purpose of the UT is to detect the charged decay products of long lived neutral particles such as $K_s^0$ and $\Lambda$. These particles live long enough to decay outside of the VELO. The UT also helps in the reconstruction of tracks in the VELO, by requiring that VELO tracks also have hits in the UT. This improves the transverse momentum resolution, reduces the rate of ghost tracks and saves computing time.

The Scintillating Fiber tracker (SciFi) is located downstream of the magnet. Previously, there were three tracking stations (T1-3), which have been replaced by three SciFi planes in Run 3. Each plane consists of four detection layers. These layers are planes made of 2.5 m long scintillating plastic fibers with a diameter of 250 µm. Four of these layers are placed consecutively, with the first and last layer having no angle with respect to the $y$-axis and the middle two layers tilted by $\pm$ 5° with respect to the $y$-axis. The ionization energy required is only a few eV, so when a particle hits the fiber, this threshold is met and optical photons are emitted. To enhance the light yield further, a fluorescent dye with matched excitation energy levels is also applied to the material.

There are two ring imaging Cherenkov counters (RICH1-2) used for particle identification (PID). These detectors identify charged particles by using Cherenkov radiation, which is emitted when charged particles travel faster than the phase velocity of light in a medium. Together with the momentum measurements from the tracking system, the mass of the particle can be determined and thus the particle type. RICH1 is located between the VELO and the UT to provide PID information for upstream tracks. RICH2 is located after the SciFi tracker and before the calorimeters and provides PID information for downstream tracks. RICH1 covers the low momentum range $\sim 1-60$ GeV/c and RICH2 covers the high momentum range $\sim$ 15 GeV/c - 100 GeV/c.

Electromagnetic and hadron calorimeters (ECAL and HCAL) are located after RICH2. The goal of the ECAL is to measure the energy of electromagnetically interacting particles. The HCAL aims to measure the energy of the heavier hadrons and to reduce the hadron background in the muon chambers. The ECAL and HCAL contain lead and iron respectively as the absorber material, which starts the showering process. Scintillator material is placed in between to measure the energy deposited in the particle shower. In front are two planes of scintillator tiles. The first layer is the Scintillating Pad Detector (SPD) and identifies if the incoming particle is charged or neutral. The second layer is the Pre-Shower (PS) detector, of which the main goal is to distinguish between electrons and charged pions. For Run 3 however, the SPD and the PS have been removed as they would be too crowded with the higher luminosity of Run 3.

In Run 3 there are four muon chambers (M2-5), which identify muons by reconstructing their tracks. Between each station is an 80 cm thick iron absorber to better separate muons from the few hadrons that are able to pass through.

### 3.2 Bremsstrahlung

One of the challenges faced by the LHCb detector is the reconstruction of the momenta of electrons and positrons due to their interaction with the detector material. When a charged particle traverses matter it can lose energy by radiative collisions, especially with nuclei. The electric field of a nucleus will accelerate and decelerate the particles as they pass, causing them to radiate photons and hence lose energy. This process of emitting braking radiation is called *bremsstrahlung* and is a particularly important contribution of the energy loss for electrons and positrons. For highly relativistic charged particles, it can be shown that that the cross-section of producing bremsstrahlung photons is of the order

$$\sigma \sim \alpha Z^2 \left(\frac{e^2}{mc^2}\right)^2,$$

where $m$ is the mass of the charged particle and $Z$ the nuclear charge [14]. Because of this inverse proportionality to mass squared, bremsstrahlung losses are much greater for electrons compared to muons. An electron track from $B^+ \to K^+ J/\psi(\to e^+e^-)$ decay typically loses $\sim 20\%$ of its momentum in bremsstrahlung [9]. This significantly lowers the reconstruction efficiency and results in poorer $q^2$ and mass resolutions.

In order to still accurately reconstruct the electron momenta, the LHCb detector attempts to 'catch' this bremsstrahlung and consequently add this energy to the momentum of the corresponding electron. For highly relativistic charged particles, bremsstrahlung is mainly emitted in the same direction as the particle's velocity. The most important bremsstrahlung losses take place in the material before and in the magnetic field, since the momentum of a particle is determined by its deflection in the magnetic field. Using the information of the particle tracks upstream and downstream of the magnet, new tracks can be extrapolated that estimate where the bremsstrahlung photons are likely to hit the ECAL. An overview of this process is shown in Fig 5.

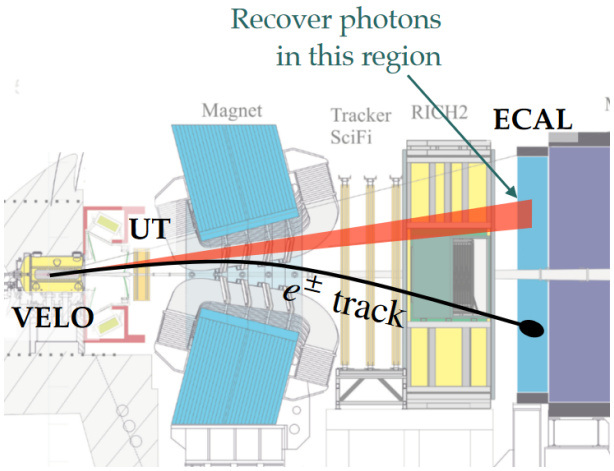


Figure 5: Schematic showing how bremsstrahlung photons emitted in the UT are caught by the ECAL, by the extrapolation of the part of the $e^{\pm}$ track before it was bent in the magnetic field [15].

# 4 Analysis & Results

In order to determine the invariant mass of $e^+e^-$ pairs, the four-momenta of the individual electrons in the $\Lambda_b^0 \to \Lambda^0 e^+e^-$ decay need to be determined. During $pp$-collisions in the LHCb detector, all kinds of $b$-hadrons are produced, which subsequently decay into more stable particles. The decay vertices, tracks, momenta and energy of these particles are then determined by the detector. After this process, various algorithms and selections are used to find the best fit for particles and tracks corresponding to various decay modes. Subsequently, the data of these candidate particles are available for analysis. In this thesis, only candidates of the $\Lambda_b^0 \to \Lambda^0(\to p\pi^-)e^+e^-$ decay, as well as its antimatter counterpart are considered.

The resolution of the invariant mass depends on the ability of the detector and algorithms to accurately reconstruct the decay processes and parameters of the particles involved. Possible errors can arise due to the mismatching of hits in the detector, possibly resulting in ghost tracks. These are tracks that do not belong to any one physical particle, but are reconstructed by the detector based on the extrapolation of consecutive hits in the detector material. Another source of error can arise due to background processes. Particles from other decays, as well as high energy radiation, can interfere with the measurement of the desired decay processes and can hence negatively influence the measurement of the energy and momentum of a particle. For electrons however, the largest impact on the resolution is the imprecise determination of their momenta, due to bremsstrahlung energy losses.

To test the global performance of the detector, Monte Carlo (MC) simulations are used. The MC consists of PYTHIA, which simulates $pp$-collisions and GeAnt4, which simulates the detector response upon measuring the particles from the simulated $pp$-collisions. The advantage of using MC data over real data is that the actual values of a particle's energy and momentum are already available to us prior to its interaction with the detector. The resolution of the invariant mass can be determined by comparing the particle's actual momentum and energy values, referred to as its 'true' values, to the values reconstructed by the detector ('rec' values). The amount by which the true and rec values deviate, gives us a direct insight into the resolution of the measurement. Using this method, the resolution of the invariant mass of the di-electron pair for both Run 2 and Run 3 can be compared.

In order to minimize effects from ghost tracks and backgrounds, the samples are filtered based on the `Lb_BKGCAT` variable. This variable is unique to the MC simulation and gives information on how the candidate $\Lambda_b^0$ particle was (mis)constructed. In the samples analysed, only data corresponding to `Lb_BKGCAT` $= 10$ or `Lb_BKGCAT` $= 50$ is used. For these categories, there is a minimum of 70% overlap between all tracks and particle types corresponding to the $\Lambda_b^0 \to \Lambda^0(\to p\pi^-)e^+e^-$ decay. The difference between these categories is that for the 50 category, extra photons were emitted during the decay in the form of final state radiation (FSR).

## 4.1 Momentum cut

In order to make the Run 3 sample more similar to the Run 2 sample, an extra selection was applied to the data. This was a cut on the true $z$-momentum of the individual electrons in the Run 3 sample. The two samples have not been through the exact same selection, so this background was only present in the Run 3 sample. In the Run 3 sample, a lot of electrons were present with a $z$-momentum lower than 1 GeV/c. The $e^+e^-$ pairs for which at least one of the electrons had $p_z < 1$ GeV/c were cut from the sample. This is a total of 1002 $e^+e^-$ pairs. Their contributions to the reconstructed invariant mass and electron momenta are shown in Fig. 6.

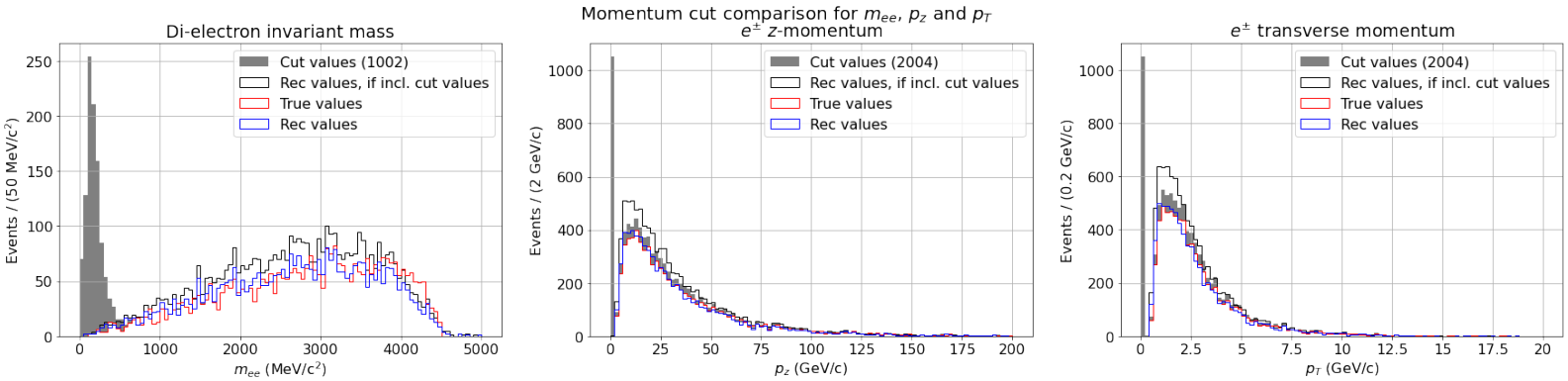


Figure 6: The di-electron invariant mass, $z$-momentum and transverse momentum, showing the case with the momentum cut applied and the case without the momentum cut applied. The rec values are sometimes higher if the cut values are included in the data, due to the momentum of the second electron in the $e^+e^-$ pair, which is often higher than the cut threshold.

This cut is however not regular background, but likely a fault in the code that is responsible for matching the true momentum to the rec momentum. This is because the reconstructed values in these graphs do not follow the same trend as the corresponding true values.

## 4.2 Reconstruction of the di-electron invariant mass

Using Eq. 4, the invariant mass of the $e^+e^-$ pairs is plotted in Fig. 4. No clear peak is observed in the invariant mass spectrum, which is as expected as there should be no other decay modes or background in the sample.

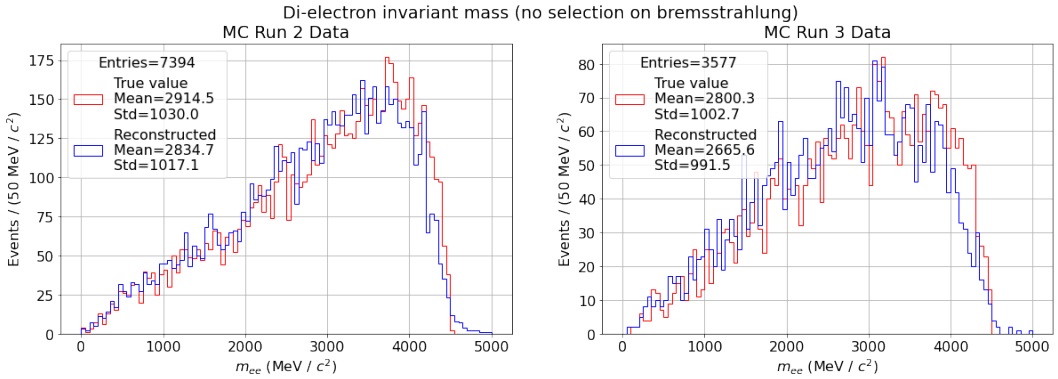


Figure 7: Invariant mass of the di-electron pair from the $\Lambda_b^0 \to \Lambda^0 e^+ e^-$ decay using MC Run 2 and MC Run 3 data, comparing the true value with the reconstructed value.

For both samples, it can be seen that in the 3500-4500 MeV/$c^2$ range, the reconstructed invariant mass is lower than the true invariant mass. This is most likely due to energy losses of the individual electrons. The MC simulation also keeps track of which electrons in the sample have gained their bremsstrahlung losses back by the bremsstrahlung recovery algorithm. To analyse this effect, the invariant mass of $e^+e^-$ pairs is determined using only pairs that have their bremsstrahlung losses added to their momenta. This is shown in Fig. 8.

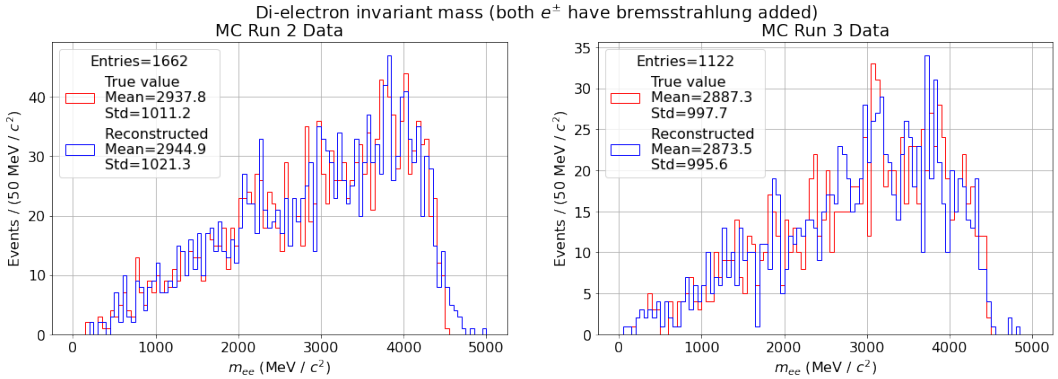


Figure 8: Invariant mass of the di-electron pair from the $\Lambda_b^0 \to \Lambda^0 e^+ e^-$ decay using MC Run 2 and MC Run 3 data, only considering electrons which have their bremsstrahlung losses added back to their momenta.

From Fig. 8, it can be observed that the true and rec invariant masses in the 3500-4500 MeV/c$^2$ range are in better agreement compared to Fig. 4. The energy losses in this range are recovered by the bremsstrahlung recovery algorithm. Also, in Fig. 8 it can be seen that the rec values have a tail between 4500 and 5000 MeV/c$^2$, whereas the true values do not. This tail is reduced in the Run 3 sample. It shows that the bremsstrahlung recovery algorithm in the Run 2 sample sometimes overestimates the momenta of $e^{\pm}$ in the reconstruction, which results in an overestimate of the invariant mass of $e^+e^-$ pairs. This has been improved in the Run 3 sample.

### 4.3 Resolution of the di-electron invariant mass

To better compare how well the invariant mass of the $e^+e^-$ pairs are reconstructed, the resolution is plotted, which is defined as

$$r(m_{ee}) \equiv \frac{m_{ee}^{\text{rec}} - m_{ee}^{\text{true}}}{m_{ee}^{\text{true}}}. \tag{5}$$

This quantity shows how much the rec and true invariant masses deviate, as a fraction of the true invariant mass. In plotting the resolution, only the data in a range from -1 to 1 are considered, as values outside this range have a large impact on the mean and standard deviation of the distribution, although they are likely misconstructed.

In addition, the data is divided into three bremsstrahlung categories, denoted BremAdded = $n$, where $n$ is the number of electrons in the $e^+e^-$ pairs that have their bremsstrahlung energy losses added back to their momenta. For instance, for BremAdded = 0, no electrons have bremsstrahlung losses added to their momenta and for BremAdded = 1, only one of the two electrons has bremsstrahlung losses added to its momentum. In Fig. 9, the invariant mass resolution of the $e^+e^-$ pairs is shown, as well as the contribution of the different bremsstrahlung categories.

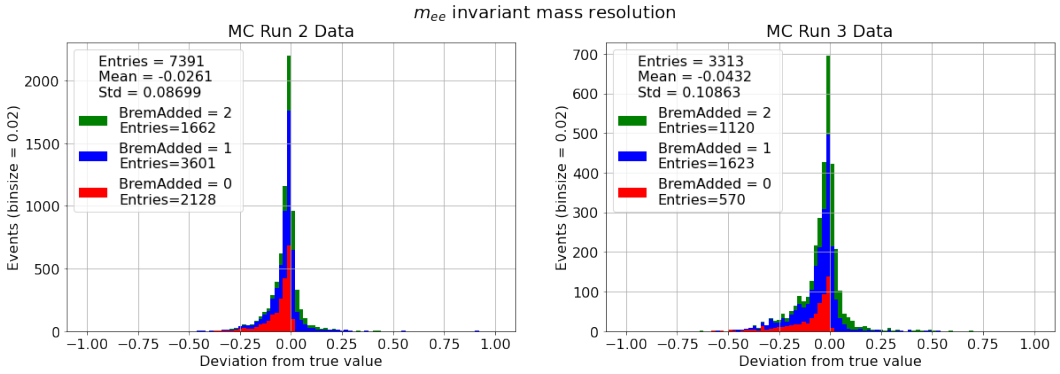


Figure 9: Invariant mass resolution of the di-electron pair from the $\Lambda_b^0 \to \Lambda^0 e^+e^-$ decay using MC Run 2 and MC Run 3 data, showing the contribution of pairs in each different bremsstrahlung category. The resolution is defined in Eq. 5.

It can be seen that there is an improvement in the recovery of bremsstrahlung losses for electrons, as the percentage of electrons in the BremAdded = 2 category is higher for Run 3 compared to Run 2. An overview of this improvement is given in the following table:

| | BremAdded = 0 | | BremAdded = 1 | | BremAdded = 2 | |
|---|---|---|---|---|---|---|
| | Entries | % of total | Entries | % of total | Entries | % of total |
| MC Run 2 | 2128 | 29% | 3601 | 49% | 1662 | 22% |
| MC Run 3 | 570 | 17% | 1623 | 49% | 1120 | 34% |

In the Run 2 sample, $\sim 47$ % of all electrons had their bremsstrahlung added to their momenta, whereas in the Run 3 sample this is $\sim 59$%. Bremsstrahlung losses have been recovered for a total of 12% more electrons in the Run 3 sample compared to the Run 2 sample.

From Fig. 9 it can be concluded that the invariant mass resolution is worse for the Run 3 sample than for the Run 2 sample. This is seen in the standard deviation, mean and in the wider shape of the graph of Run 3. From the shape, it can be seen that the Run 3 sample has a larger tail in the negative $x$-direction compared to the Run 2 sample, which is present for all three BremAdded categories. The mean of the distribution is also more negative. By taking the ratios of the means and standard deviations of both samples, it can be concluded that the mean of Run 3 is worse by a factor 1.7 and the standard deviation is worse by a factor 1.25.

The different BremAdded categories show that for electrons which do not have their bremsstrahlung losses added to their momenta, the resolution of the invariant mass is mostly negative. This makes sense, because in these cases $m_{ee}^{\text{rec}}$ is mostly lower than $m_{ee}^{\text{true}}$ due to bremsstrahlung energy losses. This is further motivated by Fig. 10, where the invariant mass resolution is plotted with respect to the different BremAdded categories.

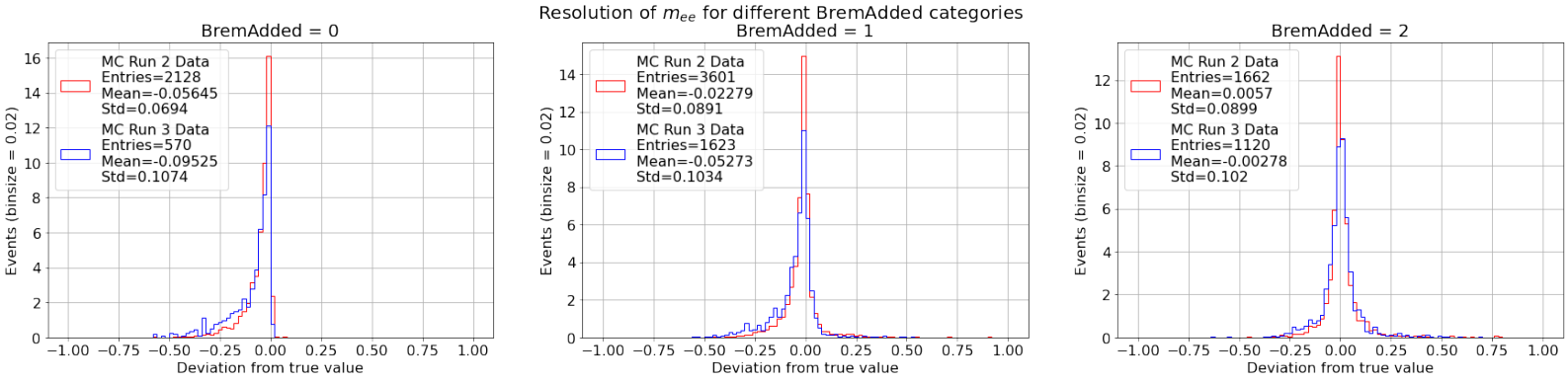


Figure 10: Resolution of the $e^+e^-$ invariant mass, as defined by Eq. 5. The resolution is divided into three bremsstrahlung categories. To compensate for the varying sample sizes, the graphs are normalised such that the area equals 1.

In Fig. 10, the mean of the distributions is negative in most cases, due to energy losses, except in the Run 2 sample in the BremAdded = 2 case. Here the mean is positive, due to the aforementioned overestimation of $e^{\pm}$ momenta by the bremsstrahlung recovery algorithm. It is also observed that the standard deviation for Run 2 gets worse for higher BremAdded categories, whereas the standard deviation for Run 3 improves. This shows that the recovery of bremsstrahlung losses results in a net higher resolution in Run 3, but deteriorates the resolution of Run 2.

It can also be seen from the BremAdded = 0 case that there are more energy losses in Run 3 compared to Run 2. In this case, no energy is recovered at all, and the mean therefore represents the average energy losses. These are higher in Run 3, as in this sample the mean is more negative. By taking the ratio of the mean values for the BremAdded = 0 case, it is estimated that the energy losses are greater in Run 3 by a factor of 1.7. However, it can be seen that the average energy losses are reduced for the BremAdded = 2 case. Also, for all categories, the standard deviation is larger for the Run 3 sample and hence the overall resolution is worse for all cases. These observations are summarized in the following table:

| | BremAdded = 0 | | BremAdded = 1 | | BremAdded = 2 | |
|---|---|---|---|---|---|---|
| | Mean | Std. | Mean | Std. | Mean | Std. |
| MC Run 2 | -0.05646 | 0.0694 | -0.02279 | 0.0891 | 0.0057 | 0.0899 |
| MC Run 3 | -0.09525 | 0.1074 | -0.05273 | 0.1034 | -0.00278 | 0.102 |
| Ratio | 1.7 | 1.5 | 2.1 | 1.2 | -0.49 | 1.1 |

## 4.4 Resolution of $e^{\pm}$ momenta

The most significant impact on the invariant mass resolution is the resolution of the momenta of the individual electrons. For highly relativistic electrons $E_e \approx p_e c$, and thus Eq. 4 can be reduced to:

$$m_{ee} = \frac{1}{c}\sqrt{2|p_{e^-}||p_{e^+}|\,(1-\cos\theta)}, \tag{6}$$

where $\theta$ is the angle between the outgoing positron and electron. Since $\theta$ is measured with higher accuracy than the momenta, the resolution of the momenta has the biggest influence on the reconstruction of the invariant mass. The distributions of the $z$-momenta of electrons for both samples are shown in Fig. 11. This is the component of the momentum parallel to the beam-axis.

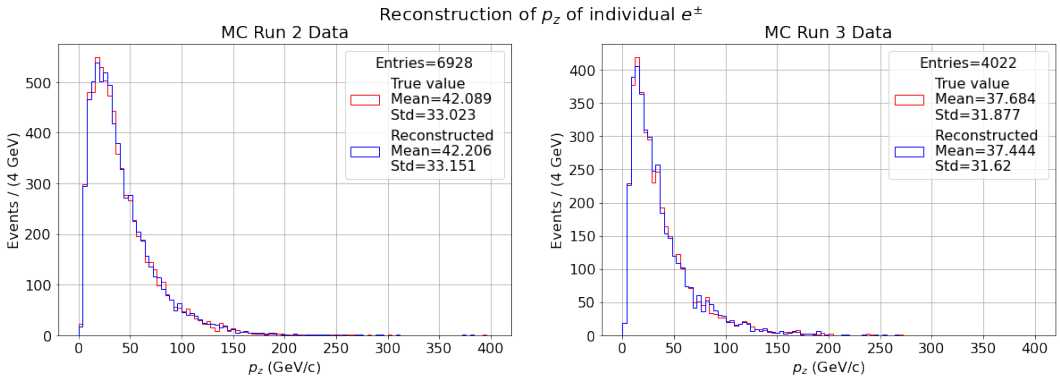


Figure 11: Distribution of $p_z$ of the individual electrons in the $\Lambda_b^0 \to \Lambda^0 e^+ e^-$ decay.

The main difference in electron $p_z$ between the two samples is that the individual electrons in the Run 3 sample have on average 5 GeV/c lower $p_z$. The shape of the distribution is also different. Run 2 has a wider peak around 40 GeV/c and Run 3 has a narrower peak around 30 GeV/c. This difference shows that although similar, the two samples do not have the same $p_z$ distribution. The resolutions of $p_z$ are shown in Fig. 12.

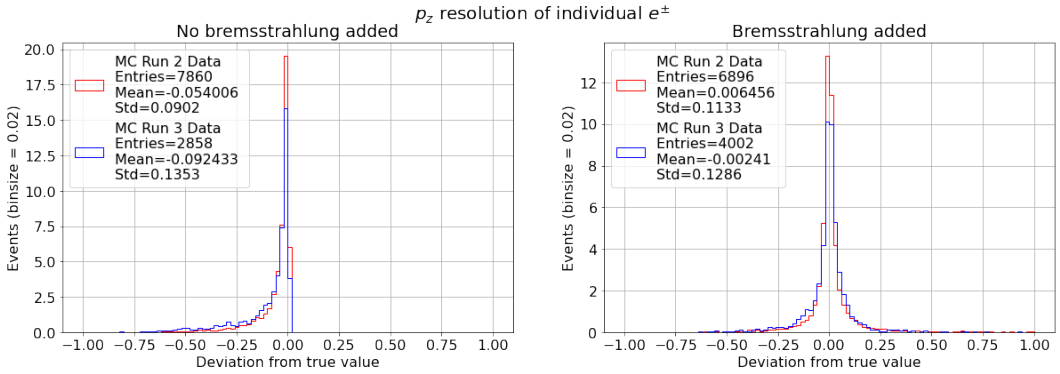


Figure 12: Resolution of $p_z$ of individual electrons. The resolution is defined in the same way as Eq. 5.

Similar to the invariant mass resolution of Fig. 10, Fig. 12 also shows that the average energy losses of the Run 3 sample are greater compared to Run 2, as for the no bremsstrahlung category, the mean of Run 3 is shifted more in the negative $x$-direction. This is also by a factor 1.7. It can also be seen that the standard deviation of the Run 3 sample is worse by a factor 1.5 when no bremsstrahlung is added and worse by a factor of 1.1 when bremsstrahlung is added, which is in agreement with the results from the invariant mass resolution. In the case where bremsstrahlung is added, the mean is shifted more towards 0 and is negative. This shows that the recovery of energy losses are better in Run 3 compared to Run 2 and that in Run 2, the bremsstrahlung reconstruction algorithm sometimes overestimates these losses.

The transverse momenta of the electrons is also analysed. The transverse momentum is the momentum that is perpendicular to the $z$-momentum (the momentum in the $xy$-plane). The distribution of $p_T$ is shown in Fig. 13.

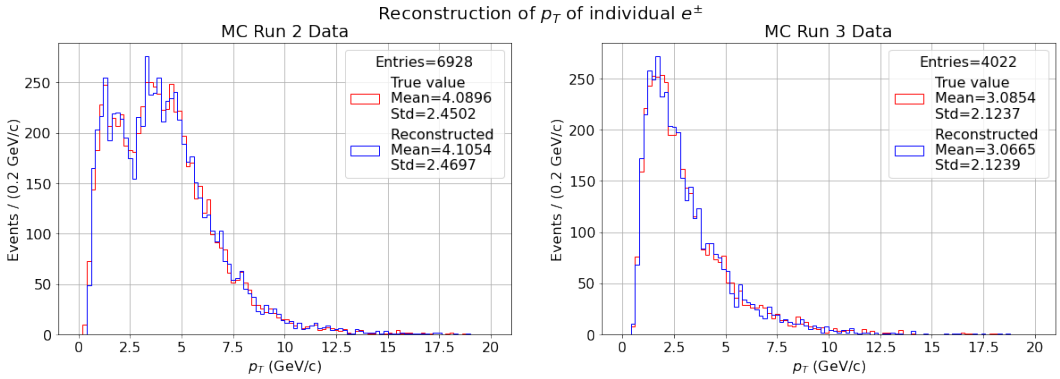


Figure 13: Transverse momentum distribution of individual $e^{\pm}$ in the $\Lambda_b^0 \to \Lambda^0 e^+ e^-$ decay.

The distribution of transverse momenta of individual electrons in Fig. 13 is different for Run 2 compared to Run 3. The main reason for this a selection of the L0 trigger. For the Run 2 sample, there is a requirement on the minimum transverse momentum of one of the two electrons in the $e^+e^-$ pair of 2.5 GeV/c. Because of this requirement, two peaks are shown for Run 2, one before and one after this threshold. Run 3 does not have this requirement and thus the distribution looks similar to the distribution of the $p_z$ momenta. To compare the accuracy of the reconstruction of the momenta, the resolution of $p_T$ is plotted in Fig. 14.

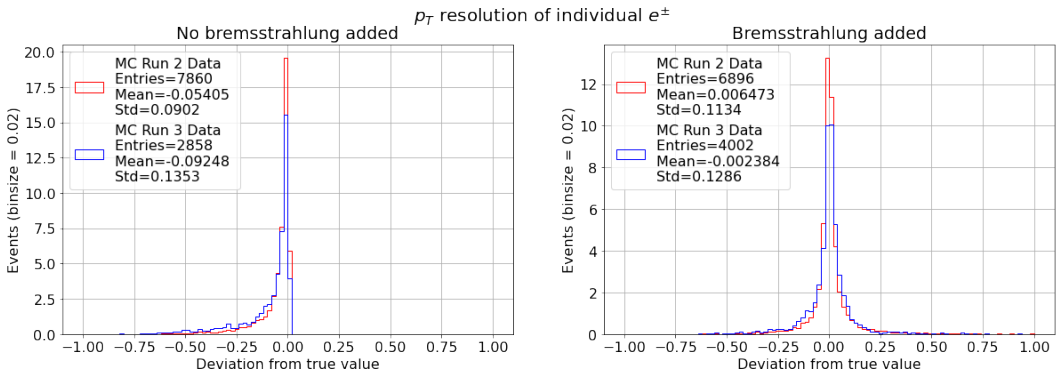


Figure 14: Resolution of $p_T$ of individual electrons. The resolution is defined in the same way as Eq. 5.

There are a lot of similarities between the resolution of $p_z$ and the resolution of $p_T$. The mean, standard deviation and shape for $p_z$ and $p_T$ resolution are almost identical, indicating that both are reconstructed with equal precision. If there was a difference in the resolution of the $p_T$ and $p_z$ momenta, it would be an interesting result and could be an indication for possible improvements. This however is not the case. These results are summarized in the following table:

| | No bremsstrahlung added | | | | Bremsstrahlung added | | | |
|---|---|---|---|---|---|---|---|---|
| | $p_T$ resolution | | $p_z$ resolution | | $p_T$ resolution | | $p_z$ resolution | |
| | Mean | Std. | Mean | Std. | Mean | Std. | Mean | Std. |
| MC Run 2 | -0.05405 | 0.0902 | -0.05401 | 0.0902 | 0.006473 | 0.1134 | 0.006456 | 0.1133 |
| MC Run 3 | -0.09248 | 0.1353 | -0.09243 | 0.1353 | -0.002384 | 0.1286 | -0.002410 | 0.1286 |
| Ratio | 1.7 | 1.5 | 1.7 | 1.5 | -0.37 | 1.1 | -0.37 | 1.1 |

$p_z$ and $p_T$ are reconstructed with equal precision, as the mean and standard deviation for both samples are the same. The shapes of the distributions do differ between the Run 2 and Run 3 samples. The resolutions of these distributions also show that there are more energy losses present in the Run 3 sample by a factor of 1.7, but that bremsstrahlung recovery has improved compared to Run 2. However, the resolution of the Run 3 sample remains worse, as the standard deviation of this sample remains higher even in the bremsstrahlung added case. These observations also arose in the invariant mass analysis, due to the high dependence on the momentum resolution.

# 5 Discussion

It is observed that the invariant mass resolution of $e^+e^-$ pairs in the Run 3 sample is worse by a factor of 1.25 compared to the Run 2 sample, based on the standard deviation. There also seem to be more energy losses by a factor of 1.7. Run 3 does however show improvements of the bremsstrahlung recovery algorithm compared to Run 2. There are 12% more electrons for which the bremsstrahlung has been recovered. In the case where bremsstrahlung is recovered, it overestimates the losses less compared to Run 2 and is on average 2.1 times more accurate. This is based on the ratio of the means of the invariant mass resolutions for the BremAdded = 2 case. Although it is on average more accurate, the standard deviation of the resolution remains worse by a factor 1.1 in this case.

In Run 3, bremsstrahlung recovery has a positive impact on the mean and standard deviation, more so than in Run 2. Still, the standard deviations remain worse in Run 3 compared to Run 2. This suggests that the deterioration of the standard deviation is not caused by the bremsstrahlung recovery algorithm. It could be that the accuracy of the rest of the tracking system is worse for Run 3. This would be by a factor of 1.25 maximally, as this is the ratio between the standard deviations of both samples. However, there are likely other effects at play that influence the standard deviation.

It is unlikely that the increase in energy losses in Run 3 are directly related to the worse standard deviation. This is because energy losses only shift all data points in the negative $x$-direction, and hence do not influence the general distribution of the data. However, it could still be that the energy losses indirectly interfere with the measurement of the $e^{\pm}$ momenta and hence influence the standard deviation.

Another factor influencing the invariant mass resolution is that the Run 2 sample and Run 3 sample have not been through the exact same selections and thus differ from each other. The biggest effect of this is seen in the different distributions of $p_T$, where the Run 2 sample has a minimum transverse momentum threshold of 2.5 GeV/c on one of the two electrons in $e^+e^-$ pairs and the Run 3 sample does not. This is not the only difference however, since the distribution of $p_z$ of individual electrons is also different for both samples. The analysis would be more representative if the distributions of $p_z$ and $p_T$ were the same for Run 2 and Run 3. It could be that the tracking system is more accurate in a certain momentum range, and hence if the momentum distributions are different, it could influence the standard deviation of the resolution. In order to achieve this, other selections can be manually applied to make the distributions in Run 2 more like the distributions in Run 3 or vice versa. An example of this is to also apply the 2.5 GeV/c threshold on the Run 3 transverse momentum.

Another sample for Run 2 was made available for analysis as well. This sample has a minimum amount of selections applied to the data, whereas the current sample of the Run 2 data has not. The analysis on the invariant mass resolution can be improved by taking the new Run 2 sample in place of the current one and observe whether the momenta distributions are more like the Run 3 sample. If this is not the case, manual selections on the momenta can be applied to make the distributions more similar. More similar momentum distributions may give a better estimate of the standard deviations.

The exact selections that cause the differences between the momentum distributions of the two samples is not known, as the reconstruction and selection algorithms operate like a 'black box'. If it is not possible to make the momentum distributions more similar, a further analysis is needed to

explain these differences and their effect on the momentum resolution.

In this analysis, not all `Lb_BKGCAT` signals were included and only `Lb_BKGCAT`=10 and `Lb_BKGCAT`=50 were used. Real data consists of a mixture of real signals, ghost tracks and other background categories and is not filtered out as easily as in the MC simulations. A more accurate analysis between the Run 2 and Run 3 samples would include all these signals. The ability of the detector to distinguish signal from non-signal is not taken into account in the current analysis, but it is a factor that influences the resolution of the invariant mass when considering real data.

Lastly a mismatching between true and rec electron momenta was found. The cause of this should be investigated further. It is possible that there are more such faults in the code used that could have impacted the results.

# 6 Conclusions

The invariant mass resolution of $e^+e^-$ pairs in the $e^+e^-$ pairs in $\Lambda_b^0 \to \Lambda^0(\to p\pi^-)e^+e^-$ decay is analysed and compared before and after the upgrade of the LHCb detector using MC simulations of Run 2 and Run 3. It was found that the invariant mass resolution of $e^+e^-$ pairs in $\Lambda_b^0 \to \Lambda^0(\to p\pi^-)e^+e^-$ is worse for Run 3 compared to Run 2 by a factor of 1.25. There were also more energy losses by a factor of 1.7. There were however improvements seen in the bremsstrahlung recovery algorithm for Run 3. 12% more electrons are reconstructed with bremsstrahlung added and their reconstruction is on average 2.1 times more accurate compared to Run 2. Although, the overall resolution of the invariant mass and momenta remains worse for Run 3. This could be caused by a lower momentum reconstruction accuracy of the upgraded tracking system, but this effect can also arise because the samples analysed do not share the same distributions for electron momenta. An analysis with similar electron distributions for Run 2 and Run 3 would give better insight into the invariant mass resolution. Lastly, a fault was discovered in the Run 3 code that generated the sample used. This fault mismatches the true and rec values of electron momenta. It is not known if more such faults are present in the code and how much they influence the result of the invariant mass resolution.

# References


[1] LHCb Collaboration. Tests of lepton flavour universality at LHCb. *Journal of Physics: Conference Series*, 1271(1), 2019.

[2] LHCb Collaboration. Test of lepton universality in beauty-quark decays. 2021.

[3] T. Blake, M. Kreps. Angular distribution of polarised $\Lambda_b$ baryons decaying to $\Lambda l^+ l^-$. *Journal of High Energy Physics*, 2017(11), 2017.

[4] ATLAS Collaboration. Observation of a new particle in the search for the Standard Model Higgs boson with the ATLAS detector at the LHC. *Physics Letters B*, 716(1):1–29, 2012.

[5] B. R. Martin, G. Shaw. *"Nuclear and Particle Physics, an Introduction" (3rd edition)*. John Wiley & Sons Ltd, 2019.

[6] R. L. Workman et al. (Particle Data Group). CKM Quark-Mixing Matrix. *Prog. Theor. Exp. Phys.*, 2022.

[7] D. Bečirević et al. Leptoquark model to explain the $B$-physics anomalies $R_K$ and $R_D$. *Physical Review D*, 94(11), 2016.

[8] A. J. Buras, J. Girrbach. Left-handed $Z'$ and $Z$ FCNC quark couplings facing new $b \to s\mu^+\mu^-$ data. *Journal of High Energy Physics*, 2013(12), 2013.

[9] P. Álvarez Cartelle et al. Test of lepton flavour universality using $B^+ \to K^+ l^+ l^-$ decays with full Run I and Run II data. 2021.

[10] LHCb Collaboration. Test of lepton universality with $B^0 \to K^{*0} l^+ l^-$ decays. *J. High Energ. Phys.*, 2017(55), 2017.

[11] A. Pattori. On the Standard Model prediction of $R_K$ and $R_{K^*}$. *Journal of Physics: Conference Series*, 770(1), 2016.

[12] J. Fuentes-Martín et al. With or without $U(2)$? Probing non-standard flavor and helicity structures in semileptonic $B$ decays. *Physics Letters B*, 800:135080, 2020.

[13] LHCb Collaboration. LHCb Tracker Upgrade Technical Design Report. 2014.

[14] H. Bethe, W. Heitler. On the stopping of fast particles and on the creation of positive electrons. *Proc. R. Soc. Lond. A*, 146(856):83–112, 1934.

[15] M. Borsato. Electron reconstruction at LHCb and Belle II. 2019.

# Appendix

The code used to reconstruct the invariant mass and the plots used in this thesis can be found here:
`https://github.com/sanderbouma/Bachelor-Research-Project.git`

The MC Run 2 dataset of the $\Lambda_b^0 \to \Lambda^0 e^+ e^-$ decay can be found here:

`/eos/lhcb/wg/RD/Lb2Lll/tuples/v4/RL/TupleProcess_EE_BDT-tau/Lb2LEE/MC18MD/Lb2LEE_procTuple.root`

The MC Run 3 dataset of the $\Lambda_b^0 \to \Lambda^0 e^+ e^-$ decay can be found here:

`/eos/lhcb/user/m/mveghel/upgradecaloreco/lb2lee/ntuples_mc_lb2lee_upgrade.root`

Packages used and their versions:

| Package | Version |
|---|---|
| Python | 3.10.4 |
| ROOT | 6.26/02 |
| Ubuntu | 22.04 LTS |
| | |
| ipykernel | 6.13.0 |
| ipython | 8.3.0 |
| jupyter-client | 7.3.0 |
| jupyter-core | 4.10.0 |
| matplotlib | 3.5.1 |
| matplotlib-inline | 0.1.3 |
| numpy | 1.22.3 |
| pandas | 1.4.2 |